Hindawi Publishing Corporation
International Journal of Antennas and Propagation
Volume 2013, Article ID 350167, 7 pages
http://dx.doi.org/10.1155/2013/350167

Research Article

Experimental UWB Propagation Channel Path Loss and Time-Dispersion Characterization in a Laboratory Environment

Lorenzo Rubio,[1] Juan Reig,[1] Herman Fernández,[2] and Vicent M. Rodrigo-Peñarrocha[1]

[1] *Electromagnetic Radiation Group (ERG), Universitat Politècnica de València, 46022 Valencia, Spain*
[2] *Escuela de Ingeniería Electrónica, Universidad Pedagógica y Tecnológica de Somagoso, Somagoso, Colombia*

Correspondence should be addressed to Lorenzo Rubio; lrubio@dcom.upv.es

Received 4 December 2012; Revised 1 March 2013; Accepted 11 March 2013

Academic Editor: Ahmed A. Kishk

The knowledge of the propagation channel properties is an important issue for a successful design of ultrawideband (UWB) communication systems enabling high data rates in short-range applications. From an indoor measurement campaign carried out in a typical laboratory environment, this paper analyzes the path loss and time-dispersion properties of the UWB channel. Values of the path loss exponent are derived for the direct path and for a Rake receiver structure, examining the maximum multipath diversity gain when an *all* Rake (ARake) receiver is used. Also, the relationship between time-dispersion parameters and path loss is investigated. The UWB channel transfer function (CTF) was measured in the frequency domain over a channel bandwidth of 7.5 GHz in accordance with the UWB frequency range (3.1–10.6 GHz).

1. Introduction

Ultrawideband (UWB) technology is defined by the Federal Communications Commission (FCC) as any wireless system that uses a large relative bandwidth in terms of the carrier frequency, typically larger than 20% or an absolute bandwidth higher than 500 MHz. Over the last decade, UWB systems have generated much interest, in both academic and industrial communities, as a consequence that the FCC assigned the 3.1–10.6 GHz frequency band (a total bandwidth of 7.5 GHz) for commercial applications in 2002 [1]. The large bandwidth occupied by UWB signals has the potentials of multipath fading resistance and high-bit-rate transmission capacity (higher than 500 Mbit/s and more for distances up to 10 m). These potentials, together with low-cost transceivers, low transmit power, and low interferences characteristics, make the UWB technology an excellent candidate for many indoor and short-range applications compared to other wireless technologies [2, 3]. Applications of UWB can be found in high data rate wireless personal area networks (WPANs), positioning, location, and home network communications related to multimedia applications [3, 4].

Given the wideband nature of UWB signals, it is of paramount importance to characterize the propagation channel properties for a flexible transceivers design and practical implementations of UWB communication systems. In this sense, many efforts and resources have been devoted in the last few years to characterize and model the UWB propagation channel. Numerous research works based on channel measurements have been reported in the literature [2, 4–8]. The measurements have been performed using both time- and frequency-domain channel sounding techniques, mainly in office, residential, in-house, and industrial environments. For understanding of measuring setups, frequency bands, and environments where the measurements were carried out, the reader can see [2, 8], as well as their references, where a large number of measurement campaigns and their results are summarized. Nevertheless, in spite of the intense research based on UWB channel measurements most of the studies reported in the open literature cover the UWB FCC band partially. For instance, only 14% of the measurement campaigns compiled in [8] have used the whole UWB FCC spectrum.

In this paper, we analyze the UWB propagation channel path loss and time-dispersion behavior in a laboratory

environment. This analysis is based on an experimental channel measurement campaign in the frequency domain covering the entire UWB FCC band designed for commercial applications, that is, the 3.1–10.6 GHz frequency band. The results reported here contribute to a better understanding of the propagation mechanisms and their effects over the transmitted signal through the UWB channel in this type of scenario. We have focused our investigation on this particular environment for the following reasons: (i) there are a lot of electronic and measurement devices which could communicate among them by a wideband technology as UWB, (ii) due to the metallic character of these devices and the rest of interacting objects, a laboratory can be considered a dense multipath scenario, and (iii) the UWB propagation channel characteristics in a laboratory environment may be different from other scenarios like indoor, office, and residential environments, where the most of measurement campaigns have been conducted.

The rest of this paper is organized as follows. Section 2 introduces the propagation environment as well as the measurement procedure and setup. Path loss and time-dispersion results are presented in Section 3. In Section 4, our results are discussed and compared with other published results. Finally, the conclusions are given in Section 5.

2. UWB Channel Measurements

2.1. Propagation Environment. The UWB channel measurement campaign was carried out in a typical laboratory, characterized by the presence of radiofrequency equipments, computers, electronic devices, metallic cupboards, tables, and chairs, among other objects. This is a dense multipath environment due to different reflection, diffraction, and scattering propagations mechanisms. The laboratory is in a modern building construction with large exterior glass windows, where the ceiling and the floor are built of reinforced concrete over steel plates with wood and plasterboards-paneled walls. Figure 1 shows the top view of the laboratory. The propagation environment consists of a 12 m-by-7 m room with a height of 2.65 m.

2.2. Measurement Procedure and Setup. The complex channel transfer function (CTF), denoted by $H(f)$, was measured in the frequency domain using a vector network analyzer (VNA), the ZVA24 of Rohde & Schwarz with a dynamic range of 140 dB up to 24 GHz and a maximum output power equal to +15 dBm. The VNA measures the S_{21}-scattering parameter which corresponds to the complex CTF. EM-6865 biconical omnidirectional wideband antennas developed by Electro-Metrics, with flat frequency response and vertically polarized, very low attenuation cables with a total length of 41 m, and two ultrawideband low noise amplifiers (LNAs), the ZX60-14012L of Minicircuits, at the receiver were also used. The transmit (Tx) and receive (Rx) antennas were placed at a height of 1.5 m above the floor. Figure 1 shows the Tx/Rx locations where the measurements were performed. For each location, the Rx antenna was set up over an XY linear positioning system emulating a 3 × 3 square grid (i.e., 9 measuring points at each receiver position), with a 4.38 cm

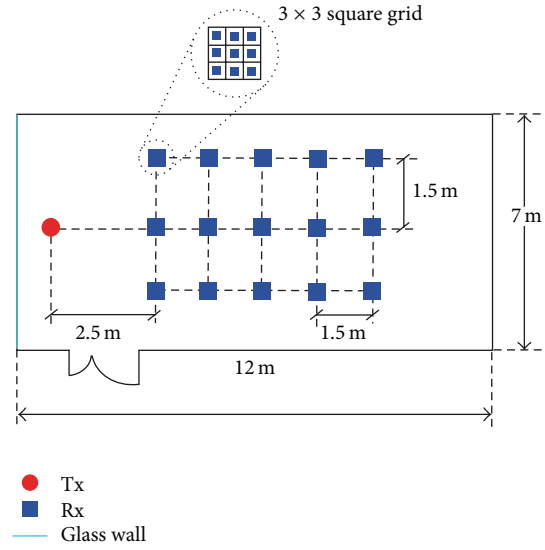

Figure 1: Top view of the propagation environment and Tx/Rx locations.

Table 1: Measurement system parameters.

Parameter	Value
VNA output power	+15 dBm
VNA SPAN (Bandwidth)	7.5 GHz
VNA center frequency	6.85 GHz
VNA IF Bandwidth	10 kHz
Average antenna gain	2.5 dB
Average LNA gain	12 dB
Antennas height	1.5 m
Total cables length	20.5 m
Cable attenuation at 3.1 GHz	0.33 dB/m
Cable attenuation at 10.6 GHz	0.64 dB/m

interelement separation, that is, the wavelength at 6.85 GHz corresponding to the central frequency of the UWB FCC band (3.1–10.6 GHz). For each position of the square grid, 100 snapshots of the complex CTF were measured at each receiver position of the square grid over a total bandwidth of 7.5 GHz (SPAN in the VNA), with 6.85 GHz as a central frequency, in order to cover the entire UWB FCC frequency band. Then, the channel impulse response (CIR), denoted by $h(\tau)$, was derived performing the inverse discrete Fourier transform (IDFT) of the measured CTF. In our case, the VNA is equipped by a time module which performs directly the IDFT, so the 100 snapshots of the CIR were recorded in a laptop. Figure 2 shows an overview of the propagation channel measurement setup and Table 1 summarizes the measurement system parameters.

A total of 15 locations were measured in line-of-sight (LOS) conditions. The minimum and maximum Tx-Rx separation distance was 2.5 and 8.65 m, respectively. The measurements were carried out at night, in absence of people, guaranteeing stationary channel conditions. Equipment calibration was performed before the measurements

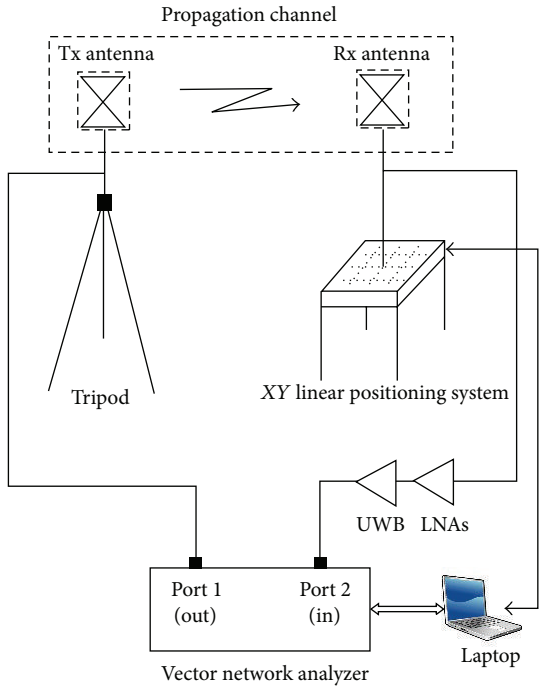

Figure 2: Overview of the frequency-domain propagation channel measurement setup.

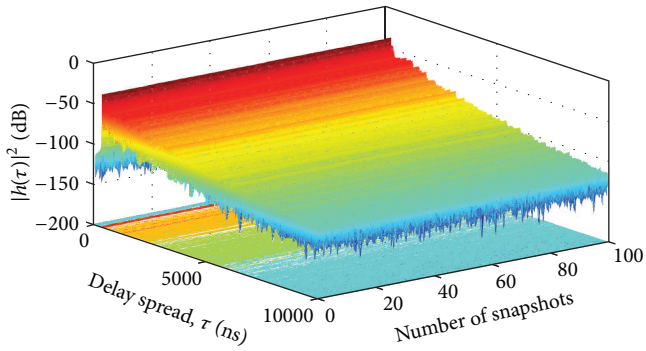

Figure 3: Measured CIR for the maximum Tx-Rx separation distance and for one position in the square grid. A total of 100 snapshots are depicted.

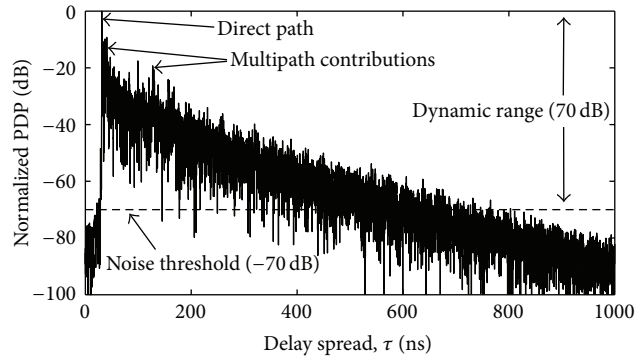

Figure 4: Normalized PDP corresponding to the CIR shown in Figure 3.

to compensate the attenuation and any imperfection of the system components, but not the antennas. Thus, the device under test (DUT) includes the radio propagation channel and the wideband antennas. Figure 3 shows the CIR measured for the maximum Tx-Rx separation distance and for one position in the square grid. A posterior average of all CIR snapshots allowed us to reduce the thermal noise, possible interferences, and minimal time variations of the propagation channel, increasing statistical analysis reliability. Thus, and assuming ergodicity, the power delay profile (PDP), denoted by PDP(τ), can be derived as PDP(τ) = $|E_k\{h_k(\tau)\}|^2$, where $E_k\{\cdot\}$ denotes expectation over all CIR snapshots for each position receiver of the square grid. Figure 4 shows the normalized PDP corresponding to the CIR of Figure 3, where a minimum dynamic range of 70 dB is achieved.

3. Measurement Results

3.1. Path Loss. Results derived from wideband and UWB channel measurements available in the literature have shown that the path loss can be related to the Tx-Rx separation distance in the same way as in narrowband channels [2, 8]. Thus, for a Tx-Rx separation distance d, the path loss in logarithmic units (dB), denoted by PL(d), can be described by the general formula

$$\mathrm{PL}(d) = \overline{\mathrm{PL}}_0 + 10\gamma \log\left(\frac{d}{d_0}\right) + S, \quad d \geq d_0, \tag{1}$$

where $\overline{\mathrm{PL}}_0$ represents the mean path loss at the reference distance $d_0 = 1$ m; the term $10\gamma \log(d/d_0)$ denotes the mean path loss referenced to 1 m; γ is the path loss exponent related to the propagation environment; and S is a zero mean Gaussian random variable, with standard deviation σ_S, used to model the large-scale fading.

Figure 5 shows the scatter plot of the path loss as a function of the Tx-Rx separation distance on a log scale for all measured data. We have distinguished the following two cases.

3.1.1. Peak Path Loss. The *peak* path loss (it is also used in the literature the term path-gain, i.e., the transmitter power divided by the average received power, that corresponds to the inverse of the path loss.), denoted as $\mathrm{PL}^{\mathrm{Peak}}(d)$, refers to the attenuation of the strongest multipath component (MPC), derived from the CIR as

$$\mathrm{PL}^{\mathrm{Peak}}(d) = \max\left\{-10\log|h(\tau, d)|^2\right\}. \tag{2}$$

It is worth noting that the new notation of the CIR introduced in (2), that is, $h(\tau, d)$, takes into account the CIR amplitude dependence on the Tx-Rx separation distance d. Due to the measurements that have been carried out in LOS conditions, $\mathrm{PL}^{\mathrm{Peak}}(d)$ is the attenuation in yhe free space of the direct path (see Figure 4). From a linear fit to the measured data using the least-squares regression procedure (solid line in Figure 5), we have observed the following values according to (1): $\overline{\mathrm{PL}}_0^{\mathrm{Peak}} = 49.65$ dB, $\gamma_{\mathrm{Peak}} = 2.04$ (≈ 2), and $\sigma_S^{\mathrm{Peak}} = 0.2663$ dB.

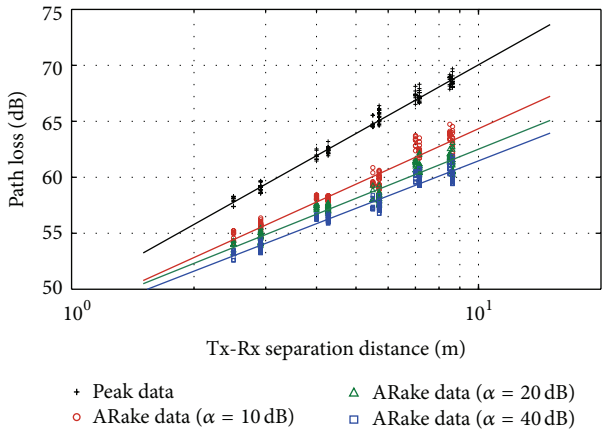

Figure 5: Scatter plot of path loss versus Tx-Rx separation distance. The solid line corresponds to the linear fit.

Table 2: ARake path loss values derived from a linear fit to the measured data in terms of the threshold level (α).

	$\overline{\text{PL}}_0^{\text{ARake}}$ (dB)	γ_{ARake}	σ_S^{ARake} (dB)
α = 10 dB	47.87	1.64	0.51
α = 20 dB	47.91	1.45	0.39
α = 40 dB	47.37	1.41	0.33

Pearsons's product moment correlation coefficient, namely linear correlation degree, denoted by ρ, is $\rho = 0.9923$ showing a linear dependence between the path loss and the logarithm of the Tx-Rx separation distance.

3.1.2. ARake Path Loss. The ARake path loss, denoted as $\text{PL}^{\text{ARake}}(d)$, refers to the total attenuation when a UWB *all* Rake (ARake) receiver capable to capture the total received energy is used. $\text{PL}^{\text{ARake}}(d)$ can be estimated from the CIR using the Parseval relation as

$$\text{PL}^{\text{ARake}}(d) = -10 \log \int_0^{\infty} |h(\tau, d)|^2 d\tau. \quad (3)$$

Notice that the ARake receiver is a Rake with unlimited correlators capable to separate all received MPCs. For a threshold (TH) level of α dB below the maximum of each PDP, equivalent to collect only the N_α MPCs that are within α dB of the strongest path (i.e., the direct path), the limits of the integral in (3) will extend to the delay interval containing the N_α MPCs. For different values of the TH level, that is, α = 10, 20, and 40 dB, Table 2 summarizes the parameter values derived from a linear fit to all measured data according to (1). We have also evaluated the ARake path loss for TH levels greater than 40 dB, and it is worth noting that no significant differences have been observed, indicating that the MPCs have negligible amplitudes. The linear correlation degree derived is ρ = 0.9522, 0.9646, and 0.9718 for α = 10, 20, and 40 dB, respectively.

For a Tx-Rx separation distance d, the maximum multipath diversity gain expected for a UWB ARake, denoted by $G_{\max}^{\text{ARake}}(d)$, can be defined by the ratio of the total energy associated all MPCs to the energy associate to the direct path. In terms of the path loss, $G_{\max}^{\text{ARake}}(d)$ can be estimated as

$$G_{\max}^{\text{ARake}}(d) = \text{PL}^{\text{Peak}}(d) - \text{PL}^{\text{ARake}}(d). \quad (4)$$

Table 3: ARake multipath diversity gain in terms of the threshold level (α).

	$G_{\max}^{\text{ARake}}(d)$	
	d = 2.50 m	d = 8.65 m
α = 10 dB	3.67 dB	5.52 dB
α = 20 dB	4.05 dB	7.17 dB
α = 40 dB	4.78 dB	8.18 dB

Table 3 summarizes the maximum multipath diversity gain in terms of the TH level and the minimum and maximum Tx-Rx separation distance. For the minimum Tx-Rx separation distance (2.5 m), the multipath diversity gain ranges from 3.67 (α = 10 dB) to 4.78 dB (α = 40 dB) whereas for the maximum Tx-Rx separation distance (8.65 m), the multipath diversity gain ranges from 5.52 (α = 10 dB) to 8.18 dB (α = 40 dB). It can be observed that multipath diversity gain increases with increasing the TH level. This is expected since more MPCs are included in the derivation of the ARake path loss when the TH level increases.

From data of Table 3, $G_{\max}^{\text{ARake}}$ increases with the Tx-Rx separation as $\beta \log(d)$, with β = 5.0, 5.9, and 6.3 for α = 10, 20, and 40 dB, respectively. Although an ARake receiver does not have a practical implementation, it corresponds to the best case and is a reference for any Rake receiver design. The number of available correlators in a receiver is usually smaller than the total number of MPCs. In this sense, the $G_{\max}^{\text{ARake}}$ should be considered as an upper bound to compare the performance of simplified Rake structures, as it is the case of a *selective* Rake (SRake) receiver, which collects the energy from the strongest MPCs, or a *partial* Rake (PRake) receiver, that only processes the first MPCs [9]. It is worth noting that the maximum multipath diversity gain values reported here are restricted to the Tx-Rx separation distances for which measured data have been taken, that is, from 2.5 to 8.65 m.

3.2. Time-Dispersion Results. Time-dispersion due to multipath propagation can limit both the transmission data rate and the capacity in multiuser UWB communication systems, and it has great impact on the UWB transceiver complexity [2, 4]. The most important parameter to characterize the time-dispersion behavior of any wireless propagation channel is the root-mean-square (rms) delay spread, denoted by τ_{rms}, which corresponds to the second central moment of the power delay profile (PDP), that can be expressed in terms of the CIR as [10]

$$\tau_{\text{rms}}(d) \triangleq \sqrt{\frac{\int_0^{\infty} (\tau - \overline{\tau}(d))^2 |h(\tau, d)|^2 d\tau}{\int_0^{\infty} |h(\tau, d)|^2 d\tau}}, \quad (5)$$

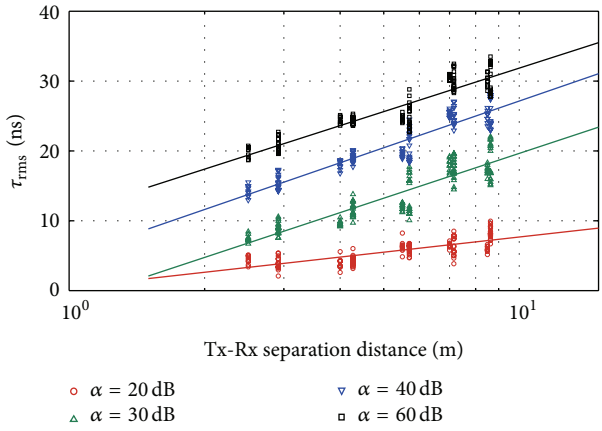

Figure 6: Scatter plot of rms delay spread versus Tx-Rx separation distance. The solid line corresponds to the linear fit.

where $\overline{\tau}(d)$ is the mean delay spread or first central moment of the PDP, given by

$$\overline{\tau}(d) \triangleq \frac{\int_0^\infty \tau |h(\tau, d)|^2 d\tau}{\int_0^\infty |h(\tau, d)|^2 d\tau}. \quad (6)$$

Figure 6 shows the scatter plot of τ_{rms} versus the Tx-Rx separation distance on a log scale for different TH levels, α = 20, 30, 40, and 60 dB. Table 4 summarizes the statistical values of τ_{rms} in terms of the TH level, that is, min., mean, max. and standard deviation (Std. dev.) values. It can be observed that τ_{rms} increases with increasing the TH level. This is expected since more MPCs are included in the derivation of τ_{rms} when the TH level increases. This observation is consistent with measurement results reported in [11]. The mean value of τ_{rms} ranges from 5.65 (α = 20 dB) to 26.06 ns (α = 60 dB). From a linear fit to the measured data (solid line in Figure 6), we can establish the following linear relationship between the mean τ_{rms} and the logarithm of the Tx-Rx separation distance:

$$\overline{\tau}_{rms}\,(\text{ns}) \simeq \tau_0 + \tau_1 \log d\,(m), \quad (7)$$

which shows a linear dependence between τ_{rms} and $\log(d)$. Table 5 summarizes the values of τ_0 and τ_1 in terms of the TH level. The linear correlation degree is ρ = 0.7609, 0.8938, 0.9281, and 0.9089 for α = 10, 30, 40, and 60 dB, respectively. Other researchers have observed a linear relationship between τ_{rms} and d, but in different propagation environments [12].

Since both delay spread and path loss increase with the Tx-Rx separation distance, a correlation between them can be expected. Figure 7 shows the scatter plot of τ_{rms} versus the path loss for a TH level α = 60 dB in both the ARake path loss and τ_{rms} derivation. From a linear fit to the measured data (solid line in Figure 7), we can establish the following linear relationship between τ_{rms} and the mean path loss ($\overline{PL}$):

$$\overline{\tau}_{rms}\,(\text{ns}) \simeq \tau_0^{PL} + \tau_1^{PL}\overline{PL}\,(\text{dB}), \quad (8)$$

where $\overline{PL}$ can be replaced by $\overline{PL}^{Peak}$ or $\overline{PL}^{ARake}$. Table 6 summarizes the values of τ_0^{PL} and τ_1^{PL} for TH levels α = 40 and 60 dB. For α = 40 dB, the linear correlation degree between τ_{rms} and the path loss is ρ = 0.9356 and 0.9598 for the $\overline{PL}^{Peak}$ and $\overline{PL}^{ARake}$, respectively. For α = 60 dB, the linear correlation degree between τ_{rms} and the path loss is ρ = 0.9140 and 0.9603 for the $\overline{PL}^{Peak}$ and $\overline{PL}^{ARake}$, respectively.

The linear correlation degree between τ_{rms} and the path loss, together with the results of Figure 7, shows that the delay spread exhibits a greater variation with the *peak* path loss. Specifically, for α = 60 dB τ_{rms} varies around its mean value with a standard deviation of 1.61 ns and 1.12 ns in terms of the *peak* and ARake path loss, respectively. Comparing the linear correlation degrees, it can be observed that the delay spread exhibits a greater correlation to the path loss than with the Tx-Rx separation distance. Although the delay spread depends on the propagation environment, this correlation behavior has also been observed in other propagation environments [8].

Table 4: Statistical values for the delay spread in terms of the threshold level (α).

	τ_{rms} (ns)			
	Min.	Mean	Max.	Std. dev.
α = 20 dB	2.09	5.65	9.93	1.66
α = 30 dB	6.70	13.67	22.05	4.17
α = 40 dB	12.95	20.91	28.38	4.19
α = 60 dB	18.28	26.06	33.50	3.98

Table 5: Parameter values of the linear delay spread model in terms of the threshold level (α).

	τ_0	τ_1
α = 20 dB	0.45	7.21
α = 30 dB	−1.66	21.31
α = 40 dB	4.92	22.21
α = 60 dB	11.16	20.68

Table 6: Statistical values for the delay spread in terms of the threshold level (α).

	Peak path loss		PRake path loss	
	τ_0^{PL}	τ_1^{PL}	τ_0^{PL}	τ_1^{PL}
α = 40 dB	−48.94	1.01	−70.21	1.58
α = 60 dB	−38.75	1.08	−60.17	1.50

4. Comparison with Published Results

Reference [8] presents a comprehensive overview of UWB channel measurements and summarizes the results derived from a great number of measurement campaigns carried out in different environments and with different measurement techniques. The results reported in [8, Table 2] show that the path loss exponent ranges from 1.3 to 2.4 in LOS conditions, with typical values on the order of 1.7, whereas higher values are reported in NLOS. The path loss exponents derived in our work when all MPCs are considered, that is, γ_{Rake} = 1.41 (α = 40 dB), and 1.45 (α = 20 dB), are

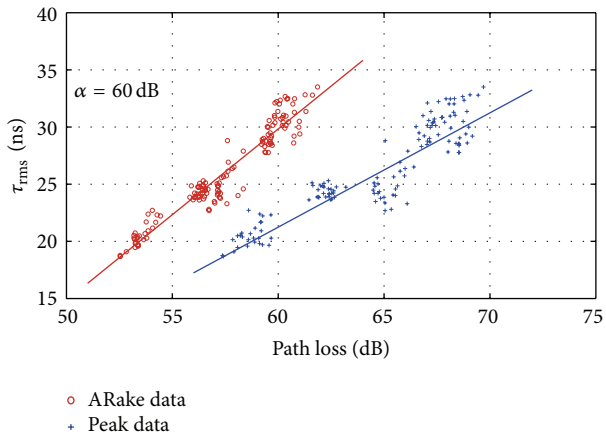

FIGURE 7: Scatter plot of rms delay spread versus path loss. The solid line corresponds to the linear fit.

less than the values reported in [8, Table 2] for laboratory environments, where values of 1.55 [11], 1.8 [13], and 1.91 [14] have been derived in LOS conditions. Low exponent path loss values have been observed in dense or multipath-rich and confined environments [15–17]. It is worth noting that the path loss exponent has a key impact on the coverage area and interference characteristics in the deployment of wireless systems; for example, low values of the path loss exponent can increase the interference [2].

The delay spread is related to the type and dimensions of the propagation environment, the radiation pattern of the antennas, and the number and electrical properties of the scatterers. Also, the estimation of τ_{rms} from the PDP increases with the noise threshold level. These dependencies make it difficult to establish comparisons among published results. Nevertheless, for Tx-Rx separation distances in the range from 5 to 30 m, indoor channels are expected to have a τ_{rms} ranging from 19 to 47 ns [18]. From our measurement campaign, the mean value of τ_{rms} ranges from 5.56 to 26.06 ns for TH levels $\alpha = 20$ and 60 dB, respectively. These mean values are in agreement with those reported in [8] for a laboratory environment in LOS conditions, where values for the average τ_{rms} of 12.3 ns for 6 m Tx-Rx separation distance are derived in [19]; 2.65 ($\alpha = 10$ dB), 9.45 ($\alpha = 20$ dB), and 15.80 ns ($\alpha = 30$ dB) for 10 m Tx-Rx separation distance are derived in [11]; and 14.3 and 19.9 ns for $\alpha = 15$ dB and the Tx-Rx separation distance ranging from 5 to 14 m are reported in [20].

As indicated in [2], the current knowledge of UWB propagation characteristics is based on a small number of measurement campaigns compared to narrowband channels. Thus, typical values of certain propagation parameters, such as the path loss exponent and delay spread metrics, only are accurate for environments with similar characteristics to those where the measurement have been collected. For a flexible transceiver design and practical implementations of UWB communications systems, more experimental studies and measurement campaigns are required, especially in particular scenarios with different propagation characteristics from office and residential environments.

5. Conclusion

In this paper, the path loss and the temporal dispersion of the UWB propagation channel have been experimentally examined for a laboratory environment. This is a dense multipath environment due to the presence of many interacting objects. The measurements were carried out in the frequency domain covering the entire UWB FCC frequency band, from 3.1 to 10.6 GHz, and for Tx-Rx separation distances in the range from 2.5 to 8.65 m. The measurements were collected in LOS conditions.

Considering a Rake structure capable to collect the total received energy, a path loss exponent equal to 1.41, 1.45, and 1.64 has been derived from all measured data for TH levels $\alpha = 40$, 20, and 10 dB, respectively. In this environment, the comparison of the *peak* and ARake path loss shows that the maximum achievable multipath gain increases with the Tx-Rx separation distance d as $\beta \log(d)$, where $\beta = 5.0$, 5.9, and 6.3 for $\alpha = 10$, 20, and 40 dB, respectively. The results show that there is a linear relationship between the rms delay spread and both the Tx-Rx separation distance and the path loss, showing a greater correlation degree with the ARake path loss. The mean values of rms derived from the measured data are 5.65, 13.67, 20.91, and 26.06 for $\alpha = 20$, 30, 40, and 60 dB, respectively.

Acknowledgments

The authors would like to thank the anonymous reviewer for his constructive suggestions and useful comments which have improved the final quality of the paper. This work has been funded in part by the Spanish Ministerio de Ciencia e Innovación (TEC-2010-20841-C04-1).

References

[1] Federal Communications Commission, "Revision of part 15 of the commission's rules regarding ultra-wideband transmission systems: first report and order," Tech. Rep. FCC 02-48, Federal Communications Commission, Washington, DC, USA, 2002.

[2] A. F. Molisch, "Ultra-wide-band propagation channels," *Proceedings of the IEEE*, vol. 97, no. 2, pp. 353–371, 2009.

[3] M. Ghavami, L. B. Michael, and R. Kohno, *Ultra Wideband, Signals and Systems in Communications Engineering*, Wiley, New York, NY, USA, 2004.

[4] I. Oppermann, M. Hamalainen, J. Linatti, and J., *UWB Theory and Applications*, Wiley, New York, NY, USA, 2004.

[5] A. F. Molisch, D. Cassioli, C. C. Chong et al., "A comprehensive standardized model for ultrawideband propagation channels," *IEEE Transactions on Antennas and Propagation*, vol. 54, no. 11, pp. 3151–3166, 2006.

[6] C. C. Chong and S. K. Yong, "A generic statistical-based UWB channel model for high-rise apartments," *IEEE Transactions on Antennas and Propagation*, vol. 53, no. 8 I, pp. 2389–2399, 2005.

[7] A. F. Molisch, J. R. Foerster, and M. Pendergrass, "Channel models for ultrawideband personal area networks," *IEEE Wireless Communications*, vol. 10, no. 6, pp. 14–21, 2003.

[8] J. Ahmadi-Shokouh and R. C. Qiu, "Ultra-wideband (UWB) communications channel measurements—a tutorial review,"

International Journal of Ultra Wideband Communications and Systems, vol. 1, no. 1, pp. 11–31, 2009.

[9] D. Cassioli, M. Z. Win, A. F. Molisch, and F. Vatalaro, "Low complexity Rake receivers in ultra-wideband channels," *IEEE Transactions on Wireless Communications*, vol. 6, no. 4, pp. 1265–1274, 2007.

[10] J. D. Parsons, *The Mobile Radio Propagation Channel*, Wiley, London, UK, 2nd edition, 2000.

[11] J. A. Dabin, A. M. Haimovich, and H. Grebel, "A statistical ultra-wideband indoor channel model and the effects of antenna directivity on path loss and multipath propagation," *IEEE Journal on Selected Areas in Communications*, vol. 24, no. 4 I, pp. 752–758, 2006.

[12] K. Siwiak, H. Bertoni, and S. M. Yano, "Relation between multipath and wave propagation attenuation," *Electronics Letters*, vol. 39, no. 1, pp. 142–143, 2003.

[13] A. Durantini and D. Cassioli, "A multi-wall path loss model for indoor UWB propagation," in *Proceedings of the IEEE 61st IEEE Vehicular Technology Conference (VTC '05)*, vol. 1, pp. 30–34, June 2005.

[14] W. Ciccognani, A. Durantini, and D. Cassioli, "Time domain propagation measurements of the UWB indoor channel using PN-sequence in the FCC-compliant band 3.6–6 GHz," *IEEE Transactions on Antennas and Propagation*, vol. 53, no. 4, pp. 1542–1549, 2005.

[15] M. G. Khan, A. A. Ashraf, J. Karedal, F. Tufvesson, and A. F. Molisch, "Measurements and analysis of UWB channels in industrial environments," in *Proceedings of the 8th International Symposium on Wireless Personal Multimedia Communications*, pp. 426–430, September 2005.

[16] C. G. Spiliotopoulos and A. G. Kanatas, "Path loss and time-dispersion parameters of UWB signals in a military airplane," *IEEE Antennas and Wireless Propagation Letters*, vol. 8, pp. 790–793, 2009.

[17] S. Chiu, J. Chuang, and D. G. Michelson, "Characterization of UWB channel impulse responses within the passenger cabin of a boeing 737-200 aircraft," *IEEE Transactions on Antennas and Propagation*, vol. 58, no. 3, pp. 935–945, 2010.

[18] J. R. Foerster, "The effects of multipath interference on the performance of UWB systems in an indoor wireless channel," in *Proceedings of the IEEE 53rd Vehicular Technology Conference (VTS '01)*, vol. 2, pp. 1176–1180, May 2001.

[19] J. Keignart and N. Daniele, "Subnanosecond UWB channel sounding in frequency and temporal domain," in *Proceedings of the IEEE Ultra Wideband Systems and Technology Conference*, pp. 25–30, Baltimore, Md, USA, May 2002.

[20] Q. Li and W. S. Wong, "Measurement and analysis of the indoor UWB channel," in *Proceedings of the IEEE 58th Vehicular Technology Conference (VTC '03)*, vol. 1, pp. 1–5, October 2003.